THE MODIFICATION OF COHERENT STRUCTURE ALONG A WAVING FILM BY POLYMER EXUDATION IN TURBULENT WATER FLOW

Yoshimichi Hagiwara
Dept. of Mechanical and System Eng., Kyoto Institute of Technology,
Matsugasaki, Kyoto 606-8585, Japan
yoshi@ipc.kit.ac.jp

Taro Imamura
Graduate student, Div. of Mechanical and System Eng.,
Kyoto Institute of Technology, Matsugasaki, Kyoto 606-8585, Japan

ABSTRACT
Direct numerical simulation and experiment have been conducted for turbulent water flow around a waving film with polysaccharide in order to examine the modification of turbulence by the exudation of the polysaccharide. The cluster models of beads, springs and dashpots are introduced near the film as representative of the entangled biopolymers. An unsteady generalized curvilinear coordinate is used for expressing the waving with solid walls. The computational results show that the population of streamwise vortices decreases near the surfaces due to the cluster models, which leads to a decrease in the shear stress. Also, it is found that the attenuation of film waving is caused by the decrease in the near-surface high-pressure regions due to the attenuation of the coherent structure.

INTRODUCTION
Some kinds of biopolymers are known to be effective for drag reduction in turbulent flow. Hoyt (1985) showed that dilute aqueous solution of some plant -, marine -, and bacterial polysaccharides reduce the friction noticeably. The application of these biopolymers to the drag reduction of ships or pipe flow in circulation systems of seawater may reduce pollution problem compared with that of synthetic polymers.

Hoyt suggested that polysaccharides are produced by algae and exuded to the surroundings for the purpose of reducing friction. Carrageenan, one of the marine polysaccharides whose effectiveness for the friction reduction has been approved, seems to be appropriate for the purpose, judging from the following reasons. Carrageenan is extracted from some species of marine red algae, and several species of these algae have large blades and small holdfasts (root-like structure). For example, *Chondracanthus exasperatus* has blades 50cm tall and 20cm wide with the holdfasts of a few centimeters in dimension (MBARI, 2000). When the velocity of tide is as high as 14-16m/s (Gaylord et al., 1994), the shear force acting on these blades becomes strong. Despite this strong shear force, the algae can be held at rocks by the holdfast and survive. It is therefere interesting to examine whether or not the exudation of Carrageenan is effective for the friction reduction.

One major difference between the blade and the solid wall in the experiment is the flexibility of the blade. The blade may wave due to the fluctuation of the surrounding flow. However, there are no experimental or computational results on the drag reduction for waving surfaces.

In the present study, we carry out direct numerical simulation for turbulent flow along a waving film with many cluster models of beads, springs and dashpots near the film surface in order to elucidate the relationship between coherent structure along a waving film and the exudation of the polysaccharide from the film. The cluster model was originally developed by our group (Hagiwara et al., 1997) as representatives of the entangled Polyethylene Oxide (PEO) measured by Miyamoto (1994).

We also conduct an experiment for turbulent water duct flow, into which a thin plastic strip covered with λ-Carrageenan powder is inserted. The images of the visualized flow and the film are processed to verify the computational result.

COMPUTATIONAL METHOD

Assumptions for film waving
It was assumed that several blades were arranged in parallel in the direction normal to the blades and that they have identical form of waving. Actually, *Chondracanthus exasperatus* has several blades connected to its one holdfast (see Fig. 1). One of the blades surrounded by the others was considered and simulated by a film.

The film displacement from its flat state was assumed to vary sinusoidally in the streamwise direction, while remaining constant in the transverse direction at any time. The positions of nodes of the sinusoidal curve were fixed on the film and in the normal direction of the film. It was also assumed that the displacement of the film at middle of two nodes was determined by the following equation:

$$\frac{d^2y}{dx^2}\left(1+\frac{dy}{dx}\right)^{-\frac{3}{2}} = -\left(\frac{\Delta p}{T}\right)\times\alpha\,,\quad \frac{dT}{dx} = -\tau_w\,, \qquad (1)$$

where x and y are the streamwise coordinate and the coordinate normal to x, Δp is the difference between the line-averaged pressure in the transverse direction at the middle of the nodes on the upper surface and that on the lower surface, and τ_w is the sum of the shear stress on both surfaces. When the numerical constant, α, is equal to 1, this equation is identical to the Young-Laplace equation for the deformation of membrane (Smith and Shyy, 1995). When $\alpha < 1$, the waving is attenuated compared with the membrane. This is equivalent to considering an elastic film with a certain thickness. α was set at 0.05 in the present study. From the measured value of Young's modulus for the blade of *Chondracanthus exasperatus* (MBARI, 2000), the film thickness was estimated to be 0.7 mm. This is comparable to the actual blade.

Computational domain

Figure 2 shows the relationship between the physical domain and the computational domain. We considered a rectangular box, in which part of the film for one period of waving was included, in the flow field (Fig. 2(a)). The streamwise dimension of the box, $2\pi h^*$, changes in time due to the film waving. The hatched area shows the lowest part of the film at this moment. The box can be converted into the domain between two parallel waving walls. The upper (lower) wall is the lower (upper) surface of the film (Fig. 2(b)). The wall configuration changes with the waving of the film.

The region between the waving walls was further converted to the channel flow region between two flat plates (Fig. 2(c)) by using the unsteady generalized curvilinear coordinates. Thus, the computational domain was a rectangular box, and the dimensions of this box ($2\pi h \times 2h \times \pi h$) were unchanged. The origin of the coordinates was at the corner of the lower wall. The ξ-, η- and z-axes were positioned in the streamwise, wall-normal and transverse directions, respectively. The domain was divided into a total of 64 × 96 × 64 cells. The cell dimension is identical either in the ξ or the z direction. It increases from the walls to the axis based on a hyperbolic tangent. The velocity components were assigned at the center of the cell surfaces (grid points for velocities), and the pressure and the external force were assigned at the center of the cell (grid points for forces). Since the amplitude of the waving was kept low, the generalized curvilinear coordinate was nearly the same as the Cartesian coordinate, and therefore, the staggered grid worked well. The Reynolds number based on h and the friction velocity for the flat plate, u^*, was 150.

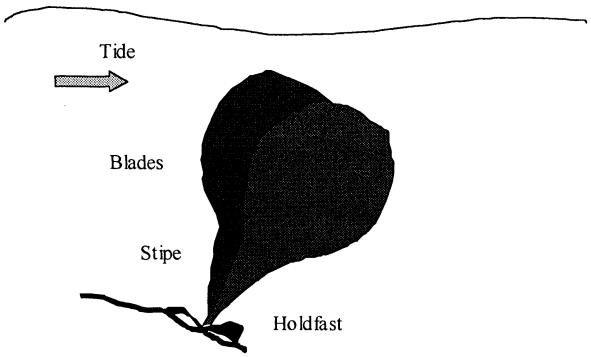

Fig. 1 : Marine red alga in see shore

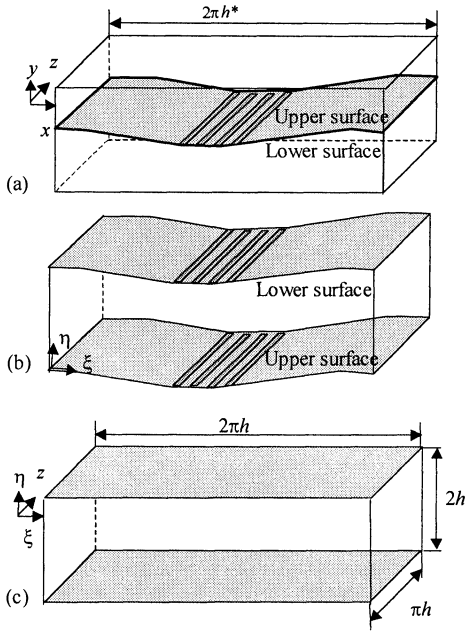

Fig. 2 : Relationship between physical domain and computational domain

Computational schemes

The second-order central difference scheme based on the interpolation method (Kawamura, 1995; Kajishima, 1994) and that without the method were applied to the finite differencing of the convection terms and the viscous terms of the momentum equations, respectively. The modified third-order Runge-Kutta method was used for the explicit time integration of the convection terms, the viscous terms and the external-force terms. The fractional-step method was adopted for the implicit time integration of the pressure terms.

Cluster model

Since we observed that λ-Carrageenan powder dissolving in quiescent water formed network structures similar to those of PEO in size, we applied the same cluster model as that used in our previous study (Hagiwara et al., 2000) as representative of the entangled polysaccharide. The nodes in the network structure of the entangled polysaccharide were replaced by beads of neutral density. The strands in

the structure were replaced by nonlinear springs of no volume. The restitution force of springs was similar to that of an FENE model, and the spring constant was identical. The interaction between the bead and the flow was dealt with as a two-way coupling: the Stokes drag force and the restitution force of the springs act on the beads, and the reaction force to the drag force acts on the flow as an external point force. The reaction force for each bead was distributed to eight neighboring grid points for forces by a spatial interpolation method. Similarly, the fluid velocity around a bead was calculated from the values at eight neighboring grid points for velocities by this interpolation method. Based on the Kelvin model, a dashpot was added in parallel with each spring to express high-viscosity due to Carrageenan. Table 1 summarizes the parameters for the present cluster model.

Whenever a bead of any cluster model reached in the region of $50 < \eta^+ < 250$, the model was removed and redefined in the region including the viscous sublayer and the lowest part of the buffer layer, in order to simulate the exudation state of polysaccharide while keeping the total number of the models constant. In this case, the height of the cluster model was reduced by two-thirds of that used in the previous study (See Table 1).

Parameters	Present	PEO
Bead radius r^+	0.3	0.5
Bead number	128	128
Spring length l^+	4.9	4.9
Spring const. k^+	0.2	0.2
Dashpot coeffi.	0.03	-
Height of model	5.5	15.7

Table 1 : Dimension of cluster model.

Initial and boundary conditions

The database of channel flow with solid walls, which was used in our previous computation, was adopted as the initial velocity field. A total of 100 cluster models were arranged uniformly near the walls for the initial condition. Half of the beads in the cluster models were allocated in the middle of the viscous sublayer, and the other half were in the buffer layer and adjacent to the sublayer.

The nonslip boundary condition was imposed for the walls. The periodical boundary condition was applied for velocity components, pressure and the cluster models in the ξ and z directions.

EXPERIMENT

Figure 3 shows the schematic diagram of the test section in the developed region of the horizontal duct of 20mm in height and 160mm in width. The apparatus including this duct is the same as that used in our previous study (Hagiwara et al, 2000).

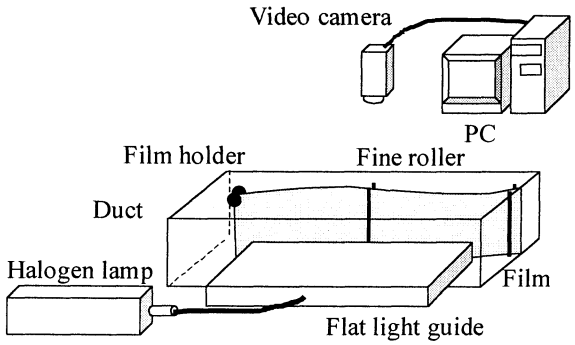

Fig. 3 Schematic diagram of test section

A thin plastic strip of 0.2mm in thickness, 14mm in width and 100mm in length was used as a waving film. The corners of the leading edge of the strip were fixed to the upper and lower duct walls by small holders (See Fig. 3). The waving of the strip in the transverse direction was restricted with fine rollers at two downstream positions so that the sinusoidal shape of the sheet was realized.

Powder of λ-Carrageenan was fixed to the surfaces of the strip using pressure before inserting the film into the flow. Bridge polymer powder, which was proven to tag to the polysaccharide for long period of time, was also fixed to the surfaces to make visible the highly entangled polysaccharide. Nylon-12 particles were mixed as tracer particles in the main water flow to measure the velocity field near the waving sheet.

Light from a halogen lamp was expanded uniformly by a flat light guide, which was made of fiber optics and a cylindrical lens. The light illuminated the powder, the tracer particles and the strip horizontally from outside the duct. The images of the reflected light from the particles and the edge of the strip were captured with a video camera located above the test section. The frame rate was 50 frames/s. A total of 1000 frames were recorded and processed with a PC. The time change in the amplitude of the waving of the strip at the middle of the film holder and the roller and the velocity vectors near the strip were obtained.

RESULTS AND DISCUSSION

Experimental result

Although the velocity vectors near the waving strip

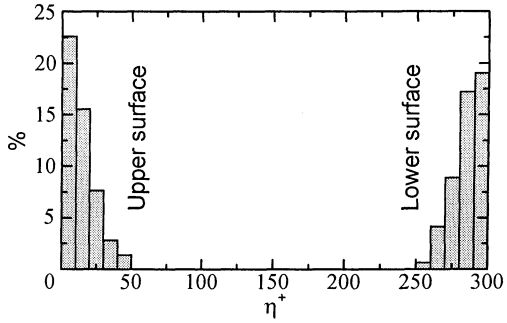

Fig. 4 : Fraction of beads

do not show a clear difference between the two cases, the maximum amplitude of the strip waving in the case with Carrageenan was about 50 % lower than in the case without the polysaccharide.

Verification of exudation state

Figure 4 demonstrates the fraction distribution of beads in the computational domain at a time. About 20 percent of the whole beads are found to be in the viscous sublayer of one side of the wall. Totally, more than 40 percent of the beads are in the viscous sublayers. Similar result was obtained in different time. It is therefore confirmed that the present method of cluster definition is effective for simulating the exudation of polysaccharide.

Turbulence statistics

The following turbulence statistics are based on the average values in the (ξ, z)-plane for the period of $1050\nu/u^{*2}$.

Mean velocity. Figure 5 indicates the mean velocity profile. In the buffer layer, the mean velocity in the case without cluster models is higher than that of solid wall. The mean velocity in the case with cluster models is lower than that without cluster models or that of solid wall. In the log region, on the other hand, the velocity in the case with cluster models is the highest among the three cases.

Turbulence intensities. Figure 6 depicts the turbulence intensities. The intensities in the case without cluster models are generally higher than those in the case of the solid wall. The intensities in the case with cluster models are lower than those in the case without cluster models or those of solid wall except for the streamwise intensity in the buffer layer.

Shear stress. Figure 7 shows the shear stress profiles. The Reynolds shear stress and the total shear stress in the case without cluster models are higher those of channel flow. These stresses in the case with cluster models are the lowest among the three cases.

Judging from Figs. 5, 6 and 7, the turbulence intensities and the Reynolds shear stress were increased by the film waving. This is because the instantaneous curve of the waving was mainly determined by the pressure difference of two surfaces at the middle of the nodes, which is not necessarily optimal for reducing the friction drag. The cluster models in the buffer layer of the waving film reduced the intensities and the shear stress. Therefore, it can be concluded that the exudation of polysaccharide is effective for the drag reduction for the waving film.

Modification of streamwise vortices

Figures 8(a) and 8(b) demonstrate the snapshot of the streamwise vortices of $\omega_x^+ < -0.2$ in light gray

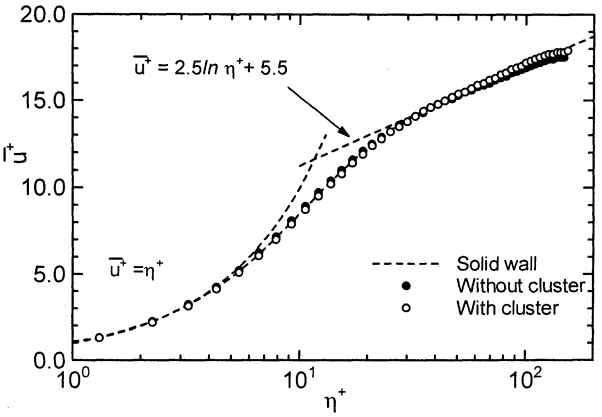

Fig. 5 : Mean velocity profile

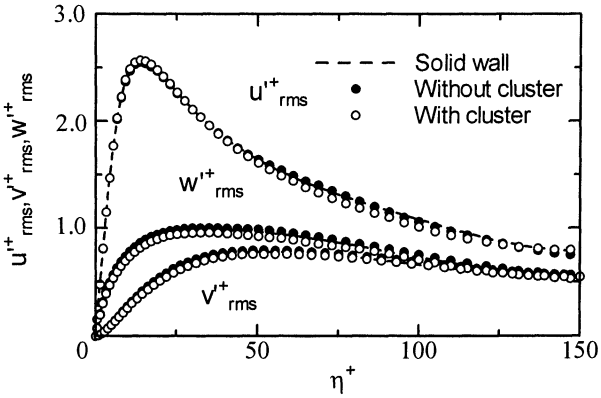

Fig. 6 : Turbulence intensities

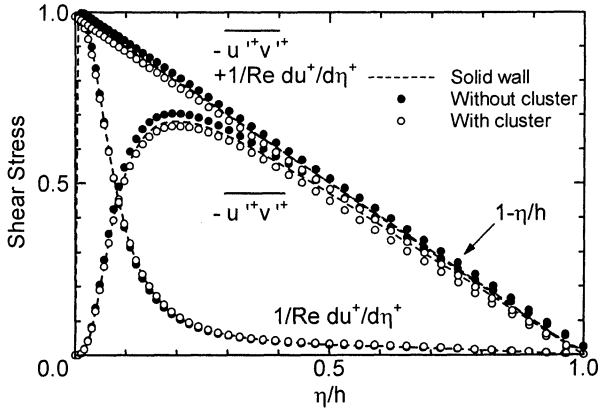

Fig. 7 Shear stress

and those of $\omega_x^+ > 0.2$ in black in the case without cluster models at $t^+ = 150$, and that with cluster models, respectively. One-eighth of the whole compututational domain is shown. Small white dots seen near the center of the domain in Fig. 8(b) are the beads of the cluster models. These dots show the elongated state of the cluster models. It is found by comparing these figures that the cluster model, which was deformed by the vortex, attenuated the streamwise vortex in black selectively. This kind of interaction was observed to continue for a period of time. Consequently, the population of the streamwise vortices decreased. This is the reason for the decreases in the Reynolds shear stress and the turbulence intensities, because the vortices play a key role in the production of the Reynolds shear

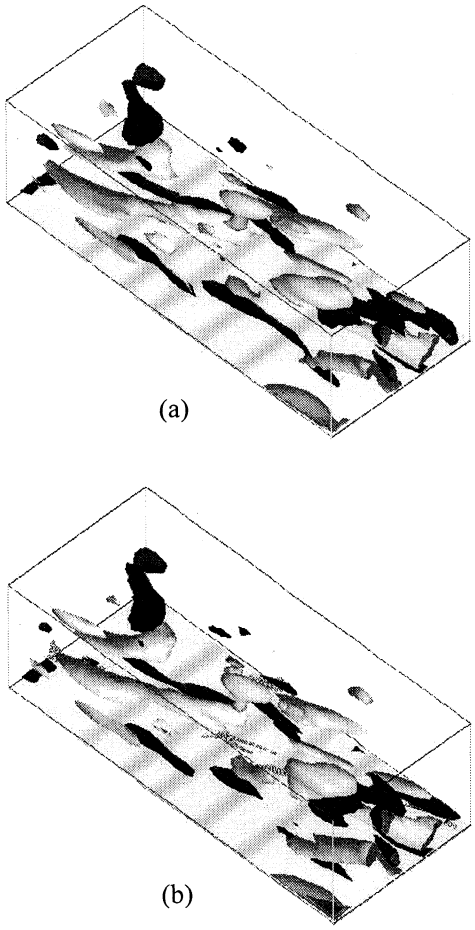

Fig. 8 : Snapshot of streamwise vortices (t^+=150)

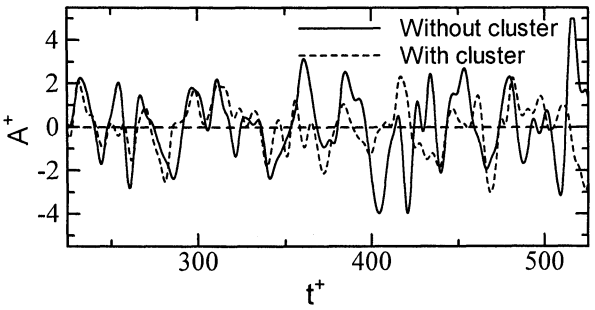

Fig. 9 : Film displacement at the middle of nodes

stress and the redistribution mechanism of the turbulent kinetic energy.

Film waving

The displacement of the film at the middle of the nodes in the case without cluster models, A^+, was 5.0 (i.e., the upper limit value), while that in the case with cluster models, A^+_c, was 3.8. The standard deviation for A^+_c was about 3 percent lower than that for A^+. It is therefore found that the cluster models attenuate the waving of the film, which is consistent with the experimental result.

Figure 9 indicates a typical example of the time changes in A^+ and A^+_c. Until t^+ = 250, A^+_c was almost identical to A^+. After that, A^+_c deviated from A^+ in most time. For some periods, such as $250 < t^+ < 270$ and $340 < t^+ < 370$, A^+_c takes higher frequencies than A^+. For some other periods, such as $380 < t^+ < 410$ and $500 < t^+ < 520$, the rate of the change in A^+_c is lower than that of A^+.

Mechanism of wave attenuation

We focus on the relationship between the near-surface coherent structures and the pressure difference between the upper surface and the lower surface, which dominates the film waving. We compare the result at t^+=390 when A^+ took a high value and was decreasing rapidly, while A^+_c was nearly equal to zero and its time change was much more gradual than that of A^+. Figure 10 indicates the velocity field in (η, z)-plane, the cross-section of the low-speed streaks in black and the profile of the pressure difference, Δp^+, in the case without cluster models. The horizontal line in Fig. 10(a) indicates the upper surface of the film (the bottom wall for the computational domain). Thus, the lower half of the plane in the computation was drawn in the upper part in this figure.

The mean value for Δp^+ in Fig. 10(b) is positive, which leads to the rapid decrease in A^+. This is mainly due to the four maximums of Δp^+ at z^+ = 75, 180, 300 and 390. Fluid impingement onto the film upper surface and the consequent bifurcation of the impinging flow into two flows along the surface are seen at the three locations except z^+ = 300. These are due to the large-scale streamwise vortices. High-pressure regions are generated on the upper surface around the stagnation point of these impinging flows (Kasagi and Shikazono, 1995). These high-pressure regions contribute the positive values of Δp^+. Note that the minimum of Δp^+ at z^+ = 260 is caused by the high-pressure region due to the stagnation near the lower surface of the film. The minimum of Δp^+ at z^+ = 340 is caused by the large-scale low-speed streak near the lower surface.

Figure 11 demonstrates the velocity field in (η, z)-plane, the cluster models in black and Δp^+. The mean value for Δp^+ in Fig. 11(b) is nearly equal to zero, which leads to the gradual change in A^+_c. The maximum for Δp^+ at z^+ = 10, and the minimums for Δp^+ at z^+ = 80 and 420 are due to the near-surface high-pressure regions associated with the flow stagnation. They cancel each other out. No other vortices, and thus the flow induced by the vortices, are observed in the central part in the transverse direction. The cluster models appearing in this region attenuated these vortices. Thus, the attenuation of the film waving is caused by the attenuation of the coherent structures by the cluster models. It can be concluded that the exudation of polysaccharide is effective for attenuation of coherent structures and drag reduction of waving film.

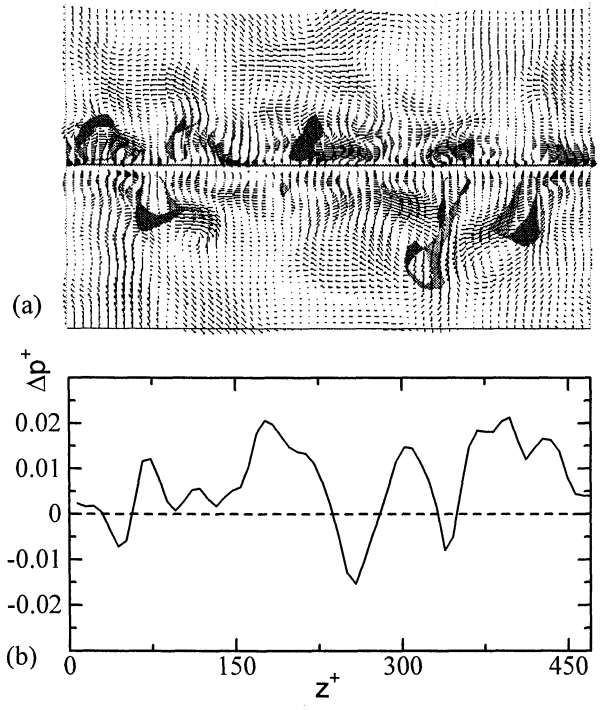

Fig. 10 : Velocity vectors in (η, z)-plane, low-speed streaks and pressure difference profile (in the case without cluster model)

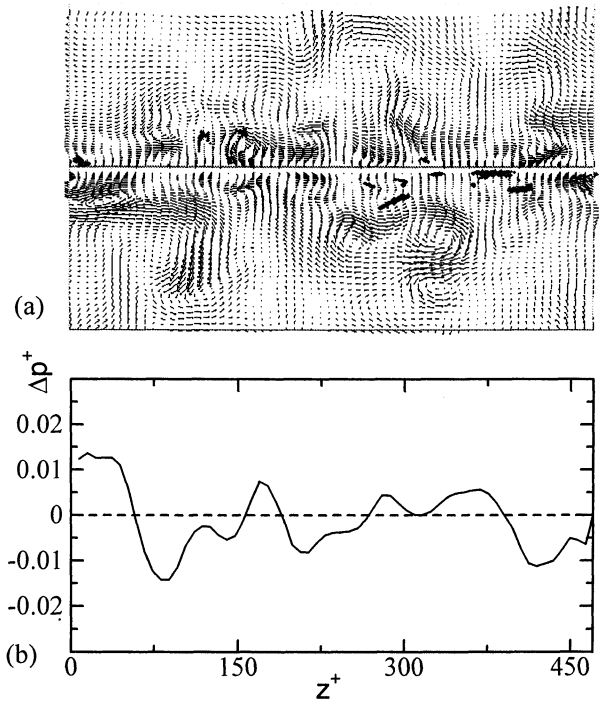

Fig. 11 : Velocity vectors in (η, z)-plane, cluster models and pressure difference profile

CONCLUSIONS

The direct numerical simulation was carried out for a turbulent flow around the waving film with many cluster models of beads, springs and dashpots representing entangled polysaccharides exuded from the film surfaces. The experiment was also done with a plastic strip covered with Carrageenan. The main conclusions are as follows.

1. The shear stress is increased by the film waving. This is because the displacement of the waving was determined mainly by the pressure difference between the upper and the lower surfaces of the film.
2. The population of streamwise vortices decreases by the presence of the cluster models near the surfaces. This kind of direct interaction leads to the attenuation of near-surface coherent structure, thus shear stress on the surface.
3. The attenuation of film waving was measured. This attenuation is caused by the decrease in the near-surface high-pressure regions, which is caused by the attenuation of the coherent structure.

The authors acknowledge the assistance of Mr. A. Taki, an undergraduate student of KIT.

References

Gaylord, B., Blanchette, C. A. and Denny, M. W., 1994, "Mechanical consequences of size in wave-swept algae", *Ecological Monographs*, vol.64, pp. 287-313.

Hagiwara, Y., Hana, H., Tanaka, M. and Murai, S., 2000, "Numerical simulation of the interactions of highly entangled polymers with coherent structure in a turbulent channel flow", *Int. J. Heat and Fluid Flow*, vol.21, pp.589-598.

Hagiwara, Y., Takashina, Y., Tanaka, M. and Hana, H., 1997, "A numerical simulation on the interaction between tangled polymers and turbulent structures", *Proc. 11th Turbulent Shear Flows*, vol. 3, pp.28-19 - 28-24.

Hoyt, J. W., 1985, "Drag reduction in polysaccaride solutions", *Trends in Biotechnology*, vol.3, pp.17-21.

Kajishima, T., 1994, "Conservation properties of finite difference method for convection" (in Japanese), *Trans. JSME (B)*, vol.60, pp.2058-2063.

Kasagi, N. and Shikazono, N., 1995, "Contribution of direct numerical simulation to understanding and modelling turbulent transport", *Proc. R. Soc. Lond. A*, vol.451, pp.257-292.

Kawamura, H., 1995, "Direct numerical simulation of turbulence by finite difference scheme", *The Recent Developments in Turbulence Research*, Int. Academic Publishers, pp.54-60.

MBARI, 2000, Home page of Montary Bay Area Research Institute, http://www.mbari.org/~conn/.

Miyamoto, H, 1994, "Experiment for visualization of polymer chains in high-polymer aqueous solutions under shear flow regions" (in Japanese), *Trans. JSME (B)*, vol. 60, pp.2038-2043.

Smith, R. and Shyy, W., 1995, "Computational model of flexible mambrane wings in steady laminar flow", *AIAA J.*, vol. 33, pp.1769-1777.